Journal of Materials Chemistry A

Facile One-Pot Synthesis of PdM (M=Ag, Ni, Cu, Y) Nanowires for use in Mixed Matrix Membranes for Efficient Hydrogen Separation

Journal:	*Journal of Materials Chemistry A*
Manuscript ID	TA-ART-12-2020-012331.R1
Article Type:	Paper
Date Submitted by the Author:	26-Apr-2021
Complete List of Authors:	Kumar, Abhishek; University at Buffalo, Department of Chemical and Biological Engineering Huang, Liang; State University of New York at Buffalo, Chemical and Biological Engineering Hu, Leiqing; University at Buffalo, Department of Chemical and Biological Engineering Yin, Deqiang; University at Buffalo - The State University of New York, Chemical and Biological Engineering Lin, Haiqing; State University of New York at Buffalo, Chemical and Biological Engineering Swihart, Mark; University at Buffalo - The State University of New York, Chemical and Biological Engineering

ARTICLE

Facile One-Pot Synthesis of PdM (M=Ag, Ni, Cu, Y) Nanowires for Use in Mixed Matrix Membranes for Efficient Hydrogen Separation

Received 00th January 20xx,
Accepted 00th January 20xx

DOI: 10.1039/x0xx00000x

Abhishek Kumar[1], Liang Huang[1], Leiqing Hu[1], Deqiang Yin[1], Haiqing Lin[1]*, Mark T. Swihart[1,2]*

Palladium (Pd) and palladium alloy nanowires (PdM; M= Ag, Ni, Cu, Y) of varying compositions were synthesized by facile and scalable one-pot polyol reduction of metallic salts using poly(vinylpyrrolidone) (PVP) as a capping agent. Alloy nanowires with a high surface area to volume ratio and an interconnected network (fractal-like) morphology may provide pathways for rapid hydrogen (H_2) transport through a mixed-matrix membrane (MMM) containing them. The use of PdM nanowires provides two benefits. First, incorporation of a metal like Ag, Cu, Y, or Ni into Pd at an appropriate level can increase the H_2 diffusivity while reducing the use of Pd. Second, alloying can reduce Pd embrittlement and susceptibility to poisoning. Polybenzimidazole (PBI) membranes loaded with PdM nanowires were prepared and tested at 150 °C and 100 psig for mixed gas H_2/CO_2 separation. MMMs containing 50 mass% pure Pd nanowires and 50 mass% $Pd_{0.75}Ag_{0.25}$ alloy nanowires showed H_2 permeabilities of 53 and 38 Barrer, which were dramatically increased from the permeability of 25 Barrer for pure PBI.

1. Introduction

Hydrogen is potentially a cost-effective and clean energy carrier that may displace fossil fuels in many future applications. Apart from being composed of the most abundant element in the universe (estimated to be around 90% of all atoms), H_2 is sustainable, non-toxic, emission-free, and has the highest calorific value of any known compounds on a gravimetric basis. The energy density of pure hydrogen is about 120 MJ/kg compared to around 42 MJ/kg for natural gas.[1] Hence, the same mass of hydrogen can provide about three times as much energy as a typical fossil fuel. More importantly, its only combustion product is water, in contrast to the CO_2, NO_x, SO_x, and other particulate matter generated from the combustion of fossil fuels. Given the advantages, the major hurdle in the widespread usage of hydrogen as a fuel is the high cost associated with its generation, purification, transport, and storage. Although scientists around the world are optimistic about hydrogen generation using renewable sources, these technologies might take another decade or more to become an economically viable alternative to fossil fuels.[2] Currently, the majority of hydrogen is produced by steam methane reforming, which produces a significant amount of CO_2 as a byproduct. If this CO_2 is simply released into the atmosphere, then the advantage of H_2 as a carbon-free fuel is largely lost. The first step in capturing CO_2 from steam reforming (or coal gasification or other syngas-producing processes) for utilization or storage is to separate the hydrogen from it. A process that keeps the CO_2 at high pressures while removing the H_2 would be advantageous for subsequent CO_2 utilization or storage. Hence, efficient hydrogen separation by transport through a membrane could reduce the cost of pure hydrogen generation as well as pave a path for CO_2 capture.

Hydrogen separation can be readily achieved using pure palladium (Pd) membranes. Palladium can reversibly absorb a large volume of hydrogen (500-1000 cm^3 per cm^3 of Pd) at ambient conditions.[3] This high volumetric sorption ability is attributed to the unique ability of Pd to selectively dissociate hydrogen at its surface and dissolve it in the form of palladium hydride (PdH_x).[4] The fact that other gases cannot dissolve in Pd ensure exceptionally high selectivity for H_2 permeation. However, pure Pd membranes have inherent disadvantages such as grain boundary defects and hydrogen embrittlement due to phase transition of Pd membranes from α to β palladium hydride at temperatures lower than 298 °C and pressures below 2 MPa.[5] Moreover, the price of Pd has skyrocketed in the past few years, making use of thicker, and therefore mechanically resilient, Pd membranes uneconomical and impractical. Pd membranes are also prone to poisoning by gases like H_2S and CO. To overcome these shortcomings, Pd is often alloyed with other transition metals to form Pd alloy-based membranes.[6] Alloying Pd with specific metals in certain stoichiometric ratios leads to an increase in permeability of membranes due to lattice expansion.[7] Several types of Pd alloy membranes, including PdCu,[8–13] PdAg,[14–17] PdAgCu,[18] PdAgNi,[19] and PdCuNi[20] have been reported in the literature with emphasis on improving

[1] *Department of Chemical and Biological Engineering, University at Buffalo, The State University of New York (SUNY)*
[2] *RENEW Institute, University at Buffalo (SUNY), The State University of New York (SUNY)*
Email : haiqingl@buffalo.edu; swihart@buffalo.edu
Electronic Supplementary Information (ESI) available: [details of any supplementary information available should be included here]. See DOI: 10.1039/x0xx00000x

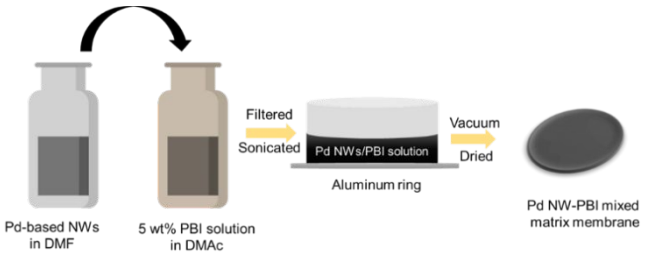

Scheme1. Schematic of steps involved in PdM NW-PBI mixed matrix membrane fabrication.

attributes such as permeability, selectivity, robustness, and resistance towards toxic gases like CO or H_2S.

Polymeric membranes that achieve H_2/CO_2 separation via size sieving provide a more practical and economical alternative to Pd and Pd alloy membranes. Hydrogen with a smaller kinetic diameter (2.89 Å) permeates through such membranes faster than CO_2 with a larger kinetic diameter (3.3 Å).[21] However, most commercial membrane materials show favorable solubility selectivity towards CO_2, which results in low to moderate H_2/CO_2 selectivity.[22] For example, the H_2/CO_2 selectivities of Matrimid®, cellulose acetates, and polysulfone (PSf) reported in the literature are 3.0, 2.5, and 2.4, respectively.[23–25] Although polymeric membranes are robust, inexpensive, and can have appreciable selectivity towards hydrogen, they often have low permeance due to the low solubility of H_2 in the membrane. Moreover, glassy polymers such as polyimides and PSf show decreased H_2 solubility at higher temperatures.[26] Among the different polymers, polybenzimidazole (PBI) membranes have been selected based on their exceptional thermal stability and their inherently high H_2/CO_2 selectivity due to their tight chain packing derived from hydrogen bonding and π-π stacking.[27] To overcome these shortcomings of Pd membranes (costly and less robust) and polymeric membranes (low permeance), mixed matrix membranes (MMMs) of Pd nanoparticles dispersed in PBI membrane have been prepared.[28,29] However, Pd-based MMMs suffer from inherent problems like void generations due to frequent volume change of Pd when transitioning from α to β phase making it less robust and prone to frequent failures.

Palladium nanowires with one-dimensional (1D) morphologies can be synthesized using solution phase methods and have certain advantages over 0D materials (nanoparticles). Specifically, they provide enhanced thermal and electrical transport properties by providing continuous pathways over relatively long distances while maintaining a high surface to volume ratio.[30] Given their anisotropic morphology and potentially better transport properties than 0D materials, 1D Pd-based materials may be a better candidate for hydrogen separation using an MMM. In this work, we report the synthesis of ultrathin wavy Pd nanowires and nanowire networks using a modified one-pot polyol synthesis procedure.[31] The synthesis process was further expanded to produce Pd alloy nanowires incorporating silver, copper, nickel, or yttrium. This is, to the best of our knowledge, the first report of the synthesis of PdNi

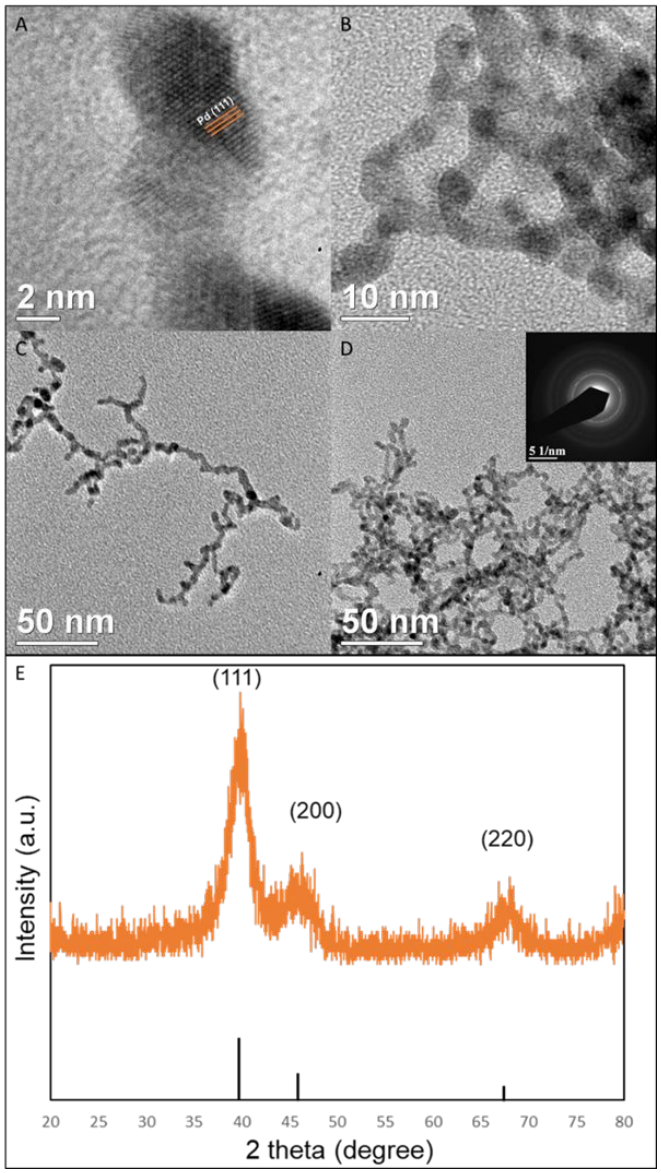

Figure 1. A-D) TEM images of Pd nanowire networks. Inset in D shows SAED patterns of Pd nanowires; **E)** XRD pattern of Pd nanowire networks

NWs by a polyol process and of PdY NWs by any process. The mechanism behind the synthesis of Pd-based nanowires is discussed, and preliminary studies of their use in MMMs for hydrogen separation are presented. Apart from reporting a facile route for the synthesis of PdM (M=Ag, Cu, Ni, Y) alloy nanowires, we report for the first time the use of Pd and Pd alloy nanowires in MMMs for H_2/CO_2 separation.

2. Experimental

2.1 Materials

Palladium (II) nitrate hydrate ($Pd(NO_3)_2.xH_2O$,≥99.9% Strem Chemicals), silver nitrate ($Ag(NO_3)$, 99%, ACROS Organics), nickel nitrate hexahydrate ($Ni(NO_3)_2.6\ H_2O$, 99%, Acros Organics), copper (II) nitrate hemi(pentahydrate) ($Cu(NO_3)_2.2.5H_2O$, ≥99.9%, Sigma-Aldrich), yttrium(III) nitrate

hexahydrate ($Y(NO_3)_3.6H_2O$, ≥99.8% , Sigma-Aldrich), poly (vinyl pyrrolidone (PVP, Mw≈29,000, Aldrich), ethylene glycol (EG, ≥99.8%, Sigma-Aldrich), N',N-dimethylformamide (DMF, Certified ACS, Fisher Scientific), and anhydrous N,N-dimethylacetamide (DMAc, >99.5%, Fisher Scientific) were used in the synthesis and processing of the NWs reported here. Celazole® PBI powder (1.1 IV grade) with Mw of 60,000 Da was obtained from PBI Performance Products, Inc. (Charlotte, SC). H_2 (99.999%), CO_2 (99.999%), N_2 and air cylinders were obtained from Airgas. All chemicals were used as received.

2.2 Synthesis of Pd nanowires

Palladium nanowires were synthesized based on a modified polyol procedure using hot injection. EG served as both solvent and reducing agent, DMF was a cosolvent, while PVP acted as a capping agent. In a typical synthesis, 100 mg of PVP was added to 10 mL EG in a three-neck flask with a Teflon-coated magnetic stir bar stirring at 600 rpm and fitted with a reflux condenser as shown in **Figure S1A**. The flask was then placed in a heating mantle with a programmable controller and heated to 170 °C with a heating rate of 20°C/min under nitrogen for one hour. Meanwhile, 20 mg $Pd(NO_3).xH_2O$ was dissolved in 5 mL DMF and sonicated (Branson 3210, 40 kHz) for approximately 30 minutes to obtain a clear solution. After one hour, the Pd solution in DMF was rapidly injected into the refluxing EG solution using a syringe. The reacting mixture was stirred at 170 °C for another hour. After the heating was stopped and the solution was cooled to room temperature, 20 mL of acetone was added to precipitate the Pd nanowires. The precipitates were collected by centrifuging the sample at 10000 rpm for 20 minutes. After centrifugation, the supernatant solution was discarded, and the sample was washed with acetone and ethanol. Finally, the sample was dispersed and stored in ethanol for further use.

2.3. Synthesis of PdM (M=Ag, Ni, Cu, Y) nanowires

PdM nanowires were synthesized using the same procedure applied for Pd nanowires. For the synthesis of PdAg, 4.25 mg of $Ag(NO_3)$ was added to 5 ml DMF along with 20 mg $Pd(NO_3).xH_2O$. The salt solution was sonicated to obtain a clear solution and then injected into the heated EG solution containing PVP. Similarly, PdNi nanowires were formed by adding 40 mg $(Ni(NO_3)_2.6\ H_2O$, PdCu nanowires were formed by adding 20 mg $Cu(NO_3)_2.2.5H_2O$, and PdY nanowires were formed by adding 6.83 mg $Y(NO_3)_3.6H_2O$ to DMF along with 20 mg $Pd(NO_3).xH_2O$. The PdM alloy nanowires were later purified following the same procedure as Pd nanowires and then dispersed in ethanol for further use. The amount of salt was determined based on the desired composition of the Pd alloy membranes used in literature for hydrogen separation and was optimized via repeated experiments.[7,32] The reported masses of salts used in synthesis are approximated based on $Pd(NO_3).xH_2O$ (~40% Pd), and the amount of other salts can be varied to obtain different compositions of PdM alloy nanowires. Because the amount of water incorporated in the Pd salt can vary and is not precisely known, the molar mass of the precursor is not precisely known. Thus, we have reported quantities in terms of mass throughout and have also given the quantities of other components in mg instead of in moles.

2.4. Preparation of Pd and PdM NWs MMMs

The prepared Pd and PdM nanowires previously dispersed in ethanol were collected by centrifugation and then redispersed in DMF to form a 20 mg/ml solution. The required amount of Pd or PdM nanowires in DMF was mixed with a PBI solution in DMAc and sonicated for 1 hour in a Quantrex® 140 sonication bath (L&R Manufacturing Company, NJ, USA). The homogenous mixture was then filtered using a 1 µm glass fiber syringe filter and sonicated again for 15 minutes. The mixture was then cast in a polished aluminum ring on a clean and leveled silicon wafer **(Scheme 1)**. The ends of the aluminum ring were sealed to the silicon wafer using a small amount of PBI solution to prevent leakage of PdM nanowires and PBI solution. The solvent was then evaporated in a 60 ^oC oven.

2.5. Characterization

The prepared PdM nanowires were characterized using a JEOL JEM-2010 Transmission Electron Microscope (TEM) at 200 kV. To prepare samples for TEM, High-Resolution Electron Microscope (HRTEM), and Selected Area Electron Diffraction (SAED), the NW dispersion were diluted further with ethanol, dropped onto a 200-mesh carbon-coated copper TEM grid from Ted Pella, and dried in a fume hood. Scanning Electron Microscopy (SEM) imaging and Energy Dispersive x-ray Spectroscopy (EDS) area scans were performed using a Cross-Beam® Focused Ion Beam-Scanning Electron Microscopy (FIB-SEM) Workstation (Carl Zeiss AURIGA) with an EDS detector (Oxford Instruments, X-Max® 20 mm^2). PdM nanowires were prepared for SEM and EDS analysis by drying samples on carbon tape. The SEM images of the PdM NWs MMMs were taken after first coating the membranes with a thin layer of gold using an SPI-Module Sputter Coater System. The X-ray Diffraction (XRD) patterns of the prepared Pd, PdM nanowires, and PdM NW/PBI MMM were obtained with a Bruker Ultima IV X-ray powder diffractometer with Cu Kα X-ray source. The Attenuated total reflection Fourier Transform Infrared (ATR FTIR) spectra of Pd-based nanowires, PVP, PBI, and PdM NW/PBI MMM were recorded using a Bruker Vertex 70 spectrometer. Finally, thermal gravimetric analysis (TGA) was used to determine the amount of PVP attached to the nanowires using an SDT Q600 thermogravimetric analyzer (TA Instruments, DE, USA) with temperatures increasing from 25 °C to 600 °C at 20 °C/min under nitrogen. Gas sorption at 150°C in PdM NW/PBI-MMM was measured using a gravimetric method with an IGA 001 microbalance (Hidden Isochema, Warrington, UK). The density of the PdM NW/PBI-MMM was determined using Archimedes' principle and a density kit-equipped analytical balance (Model XS64, Mettler-Toledo, OH).

2.5. Gas permeation measurements

For gas permeation tests, the membrane was masked on a copper disc (diameter of 47 mm, thickness of 0.003 inch, and

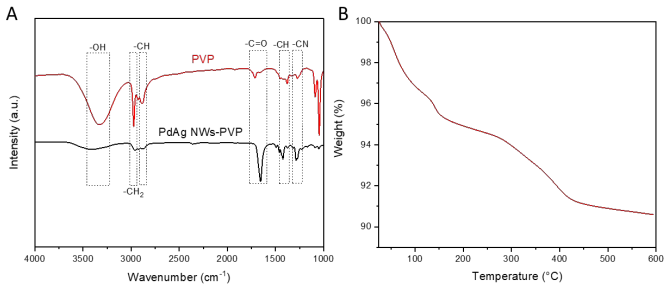

Figure 2. A) FTIR spectra of PVP and PdAg NW-PVP; **B)** TGA curve of PdAg NWs

hole for membrane of 1/4 inch to 3/8 inch) using high-temperature epoxy glue (Devcon 5 Minute® Epoxy in DevTube™) to achieve an effective area of ~0.30 cm^2. The mixed-gas permeability at 150 °C was determined using a constant-pressure and variable-volume apparatus (**Figure S1B**).[33] The feed gas flow of H_2 (100 cm^3 (STP) min^{-1}) and CO_2 (100 cm^3 (STP) min^{-1}) were controlled by SmartTrak® digital mass flow controllers (Sierra Instruments Inc., CA, US). The feed pressure of 100 psig was maintained by a backpressure regulator. N_2 (2 cm^3 (STP) min^{-1}) at atmospheric pressure was used as a sweep gas to carry the permeate gas to a 3000 Micro GC gas analyzer (Inficon Inc., Syracuse, NY, US) for composition analysis. Gas permeability (P_A) was calculated after the composition of the permeate gas became steady using the following equation:

$$P_A = \frac{x_A S l}{x_{sweep} A (p_{2,A} - p_{1,A})}$$

where S is the flow rate of the sweep gas, and x_A and x_{sweep} are the molar fraction of gas component A and sweep gas in the sweep-out gas, respectively. l is the thickness of the membrane,

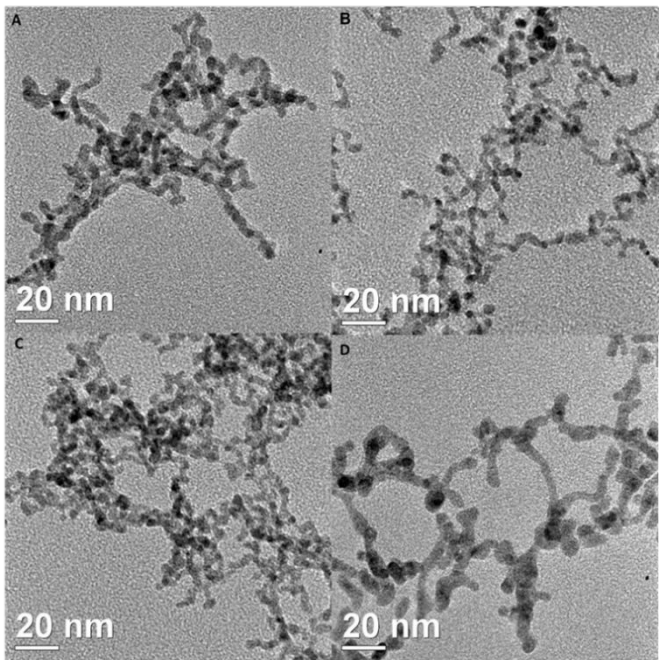

Figure 3. TEM images of **A)** PdAg nanowires **B)** PdNi nanowires **C)** PdY nanowires **D)** PdCu nanowires.

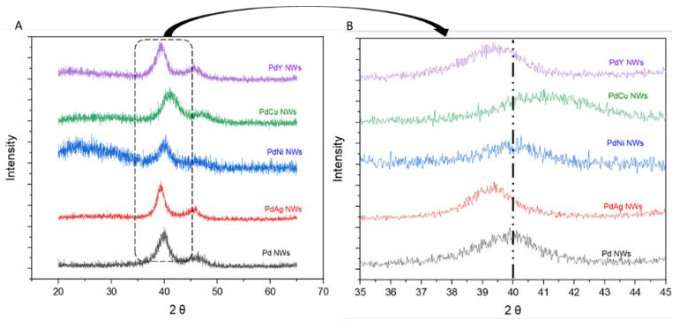

A is the effective area of the membrane, and $p_{2,A}$ and $p_{1,A}$ are the partial pressure of gas A in the feed gas and sweep-out gas, respectively.

3. Results and discussion

3.1. Pd nanowires synthesis

The morphology of the as-prepared Pd nanowires was first studied using TEM. **Figure 1(A-B)** shows TEM images of Pd nanowires, which are one-dimensional with a diameter of less than 5 nm and a typical length exceeding 200 nm. The nanowires form an interconnected network, and hence, such Pd nanowires are also called nanowire networks.[34,35] The TEM images show that the modified one-pot polyol synthesis route that we report produces a high yield of ultrathin Pd nanowire networks, with few isolated particles or other byproducts. The crystalline phase of the Pd nanowires was determined by powder XRD. **Figure 1C** shows the XRD pattern of Pd nanowires, in which the three peaks at 2θ= 40.1°, 46.7°, and 68.1° corresponding to (111), (200), (220) planes of FCC Pd, matching JCPDS card #05-0681. The broadening of the peaks is consistent with the relatively small crystallite diameter expected given the small cross-section of the Pd nanowires and their polycrystalline nature.[31] The ratio between the (111) and (200) is 2.45, and that between (200) and (220) is 1.29. This suggests that the nanowires are predominantly bounded by (111) and (110) planes, which is typical of nanowires.[36]

Figure 4. A) XRD patterns of Pd and PdM nanowires; **B)** zoomed in XRD patterns of Pd and PdM nanowires showing a shift in (111) plane peak values of corresponding nanowires

The Pd-based nanowires are synthesized using the shape controlling properties of PVP as a capping agent. During synthesis, PVP binds strongly to the facets with high surface energy, such as (100), while allowing the lower surface energy facets (111) of nanocrystals to grow to produce 1D structures.[37] To confirm the presence of PVP on the surface of synthesized Pd-based nanowires, FTIR spectra of PVP and PdAg nanowires were measured. **Figure 2A** presents the FTIR spectra of PVP and PVP-capped PdAg nanowires from 4000 to 1000 cm^{-1}. The prominent peak for PVP at 3335 cm^{-1} is attributed to the presence of -OH stretching of adsorbed water. The peaks at 2951 cm^{-1} and 2885 cm^{-1} can be ascribed to the asymmetric -CH_2 stretching and symmetric -CH_2 of the ring, respectively. The absorption band at 1644 cm^{-1} and 1279 cm^{-1} can be ascribed to

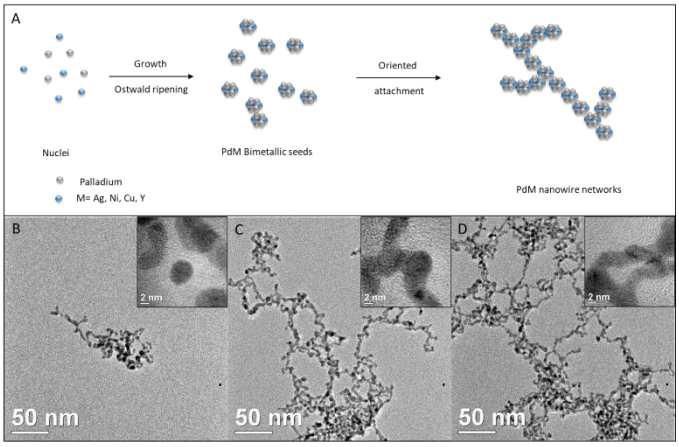

Figure 5: A) Schematic illustration of the mechanism of palladium-based alloy nanowires formation; TEM images of PdY nanowires at **B)** t=1 min, **C)** t=10 min, **D)** t=30 min (inset shows higher magnification TEM images).

the stretching vibrations of -C=O and -C-N functional groups in pyrrolidone. For the PVP-capped PdAg NWs, absorption bands for functional groups including -C=O, -C-N, -CH, and -CH_2 are still identifiable but with a slight redshift. **Figure 2B** presents a representative TGA curve of the synthesized PdAg nanowires. The TGA study was carried out in N_2 atmosphere between 25 and 600 °C with a ramp rate of 5°C. The initial mass loss of around 3% from 25 to 100 °C can be attributed to moisture loss from the nanowire surface. The mass loss of 7% is attributed to the degradation of PVP on the surface of PdAg nanowires from 100 to 400 °C after which the mass levels off.

3.2. PdM (M= Ag, Ni, Cu, Y) nanowire synthesis

The synthesis strategy for Pd nanowires was further extended to form Pd alloy nanowires. **Figure 3(A-D)** shows typical TEM images of PdAg, PdNi, PdCu, and PdY nanowires, respectively. These images show that the diameter of the nanowires was typically 4 to 5 nm, similar to that of the pure Pd nanowires. The products obtained by adding salts of Ag, Ni, Cu, and Y to Pd in DMF ultimately yielded products with the same nanowire network morphology obtained using Pd alone.

XRD patterns of the PdM nanowires show shifts in the peak positions based on the size of the alloying element. When the FCC lattice of Pd is alloyed with an atom of metal with an atomic radius smaller than that of Pd, the peaks shift to larger diffraction angles, reflecting a reduction in lattice constant. Similarly, incorporating an atom with a larger diameter into the Pd FCC crystal lattice leads to an increase in lattice constant and shifts diffraction peaks towards lower diffraction angles. The Van der Waals radii of Ni and Cu are smaller than that of Pd, whereas Ag and Y are larger than Pd.[38] From **Figure 4**, we see that the (111) peaks for PdNi and PdCu have shifted to larger angles upon the incorporation of smaller Ni[39] and Cu[40] atoms into the Pd lattice. Conversely, the addition of Ag or Y shifts the (111) peaks to smaller diffraction angles due to larger atomic radii of Ag[41] and Y.[42] Using Bragg's equation, the *d*-spacings corresponding to (111) planes for Pd, PdAg, PdNi, PdCu, and PdY were 0.225, 0.229, 0.224, 0.220, and 0.229 nm, respectively.

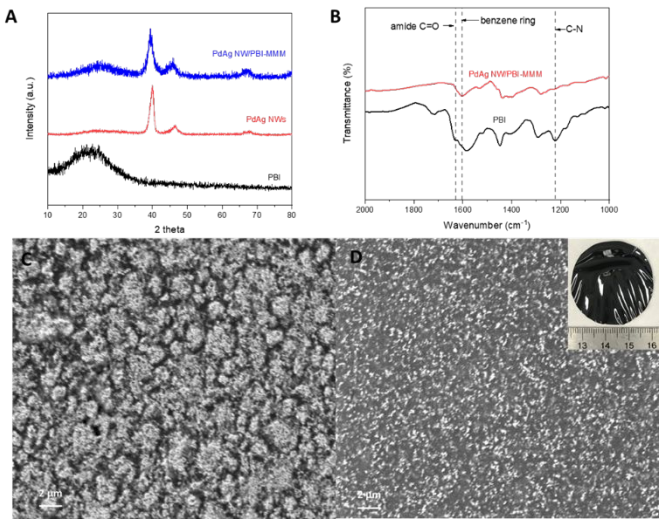

Figure 6: A) XRD patterns of PBI membrane, PdAg NWs, PdAgNW/PBI-MMM; **B)** FTIR spectra of PBI and PdAg NW/PBI-MMM; SEM images of **C)** bottom **D)** top section of PBI-PdAg NW/PBI-MMM. Inset shows the optical image of prepared PdAg NW/PBI-MMM (scale bar shows 2 µm).

These results are consistent with the substitutional incorporation of the various elements into the Pd FCC lattice. EDS analysis was used to determine the elemental composition of PdM nanowires, as shown in **Figure S2**. The approximate resulting PdM compositions were $Pd_{0.75}Ag_{0.25}$, $Pd_{0.4}Ni_{0.6}$, $Pd_{0.6}Cu_{0.4}$, and $Pd_{0.9}Y_{0.1}$. The composition of the nanowires is important for our application, as prior reports have shown that doping Pd with metals like Ag, Cu, and Y at specific concentrations increases the H_2 permeability while also making the alloy robust and resistant to poisoning in certain cases.[7] Although we limit this report to the synthesis of nanowires in a specific stoichiometric ratio for each element, in general, the PdM nanowires can be produced with other compositions and as ternary alloys by the same approach (**Figure S3)**.

3.3. PdM nanowire synthesis mechanism

The PdM nanowires grow via an oriented attachment mechanism that has been previously discussed for the synthesis of Pd nanowires.[31] To better understand the formation of PdM nanowires, the influence of reaction time on the synthesis of PdY was studied, as PdY nanowire synthesis was not previously reported by any method.[30] As soon as the salt solution of Pd and Y in DMF was injected into refluxed EG, the solution instantly became black, suggesting a rapid burst of particle nucleation. Aliquots were then extracted from the three-neck flask at different reaction times. **Figure 5** shows TEM images of PdY nanowires obtained after different reaction times. The TEM image of a sample extracted immediately after injecting the metal salt solution shows small nanoparticles with diameters of 2-3 nm. This observation suggests that the initial kinetics of Pd reduction are fast. The resulting Pd or PdY seeds have high surface energy, which drives aggregation to reduce the overall surface energy of the system and form nanowires bounded by the lowest energy facets {111}. It was further confirmed by our

XRD results, which showed that the nanowires have a high-intensity peak of (111) plane. Our time-dependent study and XRD results led us to propose a mechanism for PdM nanowires, which can be summarized in **Figure 5**.

3.4. Gas permeation property of mixed matrix membranes (MMMs)

The synthesized Pd and Pd-based nanowires were used to fabricate MMMs with PBI. For sake of demonstration, the PdAg NW/PBI-MMM was characterized in detail, but we expect other PdM NW/PBI membranes to show similar results. **Figure 6A** presents XRD spectra of the synthesized PdAg NW/PBI MMM, PdAg NWs, and pure PBI membranes. The XRD of PdAg NW/PBI MMM shows peaks corresponding to both PdAg NWs and PBI membranes. The diffraction peak of PBI in PdAg NW/PBI-MMM is 25° as compared to 22° for pure PBI. Furthermore, the corresponding *d*-spacing changed from 4.0 Å for pure PBI membranes to 3.6 Å in PdAg NW/PBI-MMM. This could be due to strong interactions between PBI and PVP-capped PdAg NWs. **Figure 6B** presents the FTIR spectra of PBI and PdAg NW/PBI-MMM. The characteristic peaks corresponding to benzene rings and tertiary amides (-C=O vibrations and C-N vibrations) can be seen at 1603, 1630, and 1225 cm^{-1}, respectively, for both PBI and PdAg NW/PBI-MMM.[37]

Table 1: Summary of mixed-gas H_2/CO_2 separation properties at 150 °C

NWs in MMMs		P (H_2) (Barrer)	P (CO_2) (Barrer)	H_2/CO_2 selectivity
Type	Loading (wt.%)			
None	0	25	2.1	12
$Pd_{0.75}Ag_{0.25}$ NW	25	32	4.2	7.7
$Pd_{0.75}Ag_{0.25}$ NW	50	38	4.2	8.9
$Pd_{0.4}Ni_{0.6}$ NW	50	32	3.6	8.9
$Pd_{0.92}Y_{0.08}$	50	60	10.5	5.8
Pd NW	25	52	9.9	5.2
Pd NW	50	53	8.1	6.4

Figure 6(C-D) presents SEM images of the top and bottom surfaces of typical MMMs. The bottom part of the PBI-PdNW MMM has a higher concentration of Pd nanowires, which we attribute to aggregation and settling of Pd NWs during solvent evaporation. Nonetheless, the NWs formed an interconnected network of thin worm-like nanowires. The inset in **Figure 6D** presents an optical image of the synthesized MMM with a thickness of approximately 30 µm. To determine elemental distribution of the prepared membrane, EDS and corresponding elemental image of the top (**Figure S4**) and bottom (**Figure S5**) PdAg/PBI-MMM were also obtained. From the EDS results, we observed that the ratio of C: PdAg at the surface was 15.90, as compared to C: PdAg of 11.69 at the bottom surface. This indicates a higher amount of PdAg nanowires at the bottom of the PdAg-MMM. This difference is also visible in the SEM images. On the length scale of elemental mapping in the SEM,

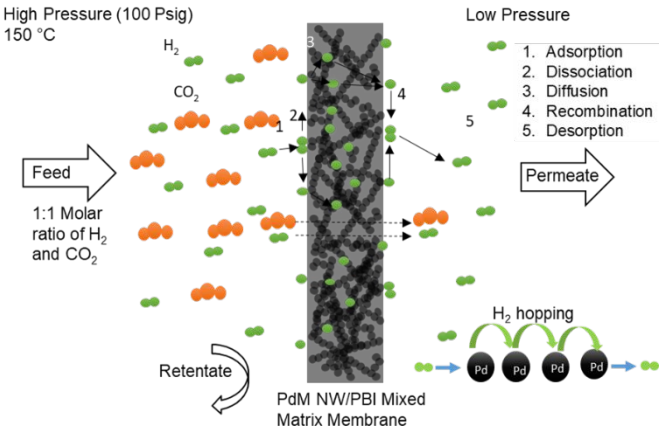

Figure 7: Schematic of hydrogen separation mechanism in a PdM NW-PBI mixed matrix membrane

the PdAgNWs are uniformly distributed in the plane of the membrane.

The prepared PBI-PdMNW MMMs were tested for hydrogen separation at 150°C and 100 psig with the feed gas mixture of H_2/CO_2 (50/50), and the separation results are summarized in **Table 1**. A pure PBI membrane prepared without any nanowires was used as a control in this experiment. The H_2 permeability of PdNW-PBI MMM (50 wt% Pd NWs) increased by more than 100% from 25 Barrer (1 Barrer = 10^{-10} cm^3 (STP) cm cm^{-2} s^{-1} $cmHg^{-1}$) for pure PBI to 53 Barrer. However, we also observed an increase in permeability of CO_2 from 2.1 Barrer for the pure PBI membrane to 8.1 Barrer. This led to a decrease in the selectivity of MMM to 6.4, compared to 12 for the pure PBI membrane. The increase in H_2 permeability was found to depend upon the amount of NWs used in the membrane. A membrane containing 25 wt% $Pd_{0.75}$ $Ag_{0.25}$ nanowires had a H_2 permeability of 32 Barrer, and permeability increased to 38 Barrer upon increasing the amount of $Pd_{0.75}$ $Ag_{0.25}$ NWs in the MMM to 50 wt%. Similar results were obtained using $Pd_{0.4}Ni_{0.6}$ nanowires to make PdNi-PBI MMMs. A 50 wt% mixture of $Pd_{0.4}Ni_{0.6}$ and PBI showed a H_2 permeability of 32 Barrer with a selectivity of 8.9, and $Pd_{0.92}Y_{0.08}$ NW-PBI MMM shows permeability of 60 Barrer with a selectivity of 5.8 **Figure S6** shows the separation performance of the PdM NW/PBI-MMMs in comparison with Robeson's 2008 upper bound at 150 °C. This decrease in the selectivity of PdM-MMMs could be due to two probable reasons. First, the nanowires are prepared using PVP (Mw≈29000) as a ligand, which is a long-chain polymer that may generate imperfections within the MMMs. Secondly, the nonuniform dispersion of Pd NWs through the membrane due to agglomeration and sedimentation of nanowires degrades performance, which is a widely known problem in MMMs.[43]

The H_2 permeation in a PdNW-PBI MMM occurs through a multi-phase solution-diffusion mechanism. The membrane is composed of a PdNW network dispersed throughout the PBI phase. In the PBI phase, transport is by the solvation

(absorption) of H_2 in the polymer, diffusion, and desorption. However, transport through the Pd phase involves diffusion of H atoms, rather than H_2 molecules. Transport through Pd can be described as a sequence of 5 processes: adsorption, dissociation, diffusion, recombination, and desorption. H_2 transport through the Pd phase can start with its adsorption and dissociation on exposed Pd nanowires at the surface of the membrane. Hydrogen atoms may then diffuse to the other side of the membrane through the continuous network provided by nanowires within the membrane matrix, where they recombine and desorb as H_2. However, H_2 dissolved in the PBI matrix can also dissociate upon coming in contact with PdNWs within the membrane, and H atoms dissolved in Pd can recombine at the PdNW/PBI interface. Because for a given H_2 partial pressure, the equilibrium concentration of H atoms in Pd is much greater than the equilibrium concentration of H_2 in PBI, hydrogen preferentially partitions into the Pd (or PdH_x) phase, accelerating its transport through the MMMs resulting in enhanced hydrogen separation.

These pathways can occur in parallel and/or in series. In Pd nanoparticle-based MMMs without continuous paths through the membrane, transport of hydrogen involves a hopping mechanism that requires multiple dissociation-recombination processes as H atoms move from one Pd nanoparticle to another within the membrane matrix.[28] Pd nanowires may provide a continuous network through the membrane for rapid transport of H atoms with fewer dissociation and recombination events. In polymeric membranes, H_2 and CO_2 gas permeability (P_{H2} and P_{CO2}) are each directly proportional to a solubility coefficient (S_{H2} and S_{CO2}) and a diffusion coefficient (D_{H2} and D_{CO2}). Hydrogen has higher diffusivity than CO_2 because of its smaller kinetic diameter (2.89 Å) than CO_2 (3.3 Å). However, solubility selectivity favors CO_2 due to its higher condensability.[21,44] Hence, in a PdNW-PBI MMM, CO_2 transports through PBI by dissolution, diffusion, and desorption but not through the Pd phase, as CO_2 cannot be dissolved in Pd. In addition to transport through PBI, both H_2 and CO_2 can be transported through defects in the membrane, and both may be transported through the PVP adsorbed on the Pd nanowire surfaces, in both cases at different fluxes from those through PBI. If defects behave as small pores, then the permeability by that route would not be governed by a solution-diffusion mechanism, but by simple Knudsen diffusion, for which the selectivity depends only upon the molar mass of the diffusing species. Knudsen diffusion gives a H_2/CO_2 selectivity of approximately 4.7. If transport through defects and through PVP could be fully eliminated, we would expect the CO_2 permeability to decrease with increasing Pd content, as observed in our prior work with Pd nanoparticles dispersed in PBI.[28] The mechanism of H_2 separation through a PdNW-PBI MMM is summarized in **Figure 7**. To test this proposed mechanism based on enhanced H_2 sorption in the MMMs, H_2 sorption in the PdAg NW/PBI-MMM was determined at 150°C. **Table S1** summarizes H_2 sorption and solubility of PdAg NW/PBI-MMM at 150 ℃ and varying pressures. At 11.4 bar, the PdAg NW/PBI-MMM has H_2 sorption of 34 cm^3(STP) cm^{-3} and a solubility of 3.0 cm^3(STP) cm^{-3} atm^{-1}, which is significantly higher than that of polymers used in hydrogen separation.[26]

4. Conclusions

We report a simple one-pot polyol synthesis route to produce Pd and PdM (M= Ag, Ni, Cu, Y) nanowires. Of these PdY and PdNi alloy nanowires were not previously synthesized using the polyol method. Further, we demonstrate, for the first time, the application of Pd and Pd alloy (PdAg and PdNi) nanowires for hydrogen separation in mixed matrix membranes. The Pd and PdM NW-PBI MMMs showed higher hydrogen permeability than pure PBI membranes, paving the way for future application of nanowires as channels for gas transport within MMMs. The use of Pd alloy nanowires instead of pure Pd nanowires will help in reducing the cost of membranes, increasing permeability, and forming hysteresis-free membranes that will prevent the formation of defects in MMMs on continuous use. Future work should focus on improving membrane fabrication and elimination or replacement of high molecular weight ligands like PVP with oleylaime or hexadecyl amine to maintain H_2/CO_2 selectivity as H_2 permeability is increased by nanowire incorporation.

Conflicts of interest

The authors declare no conflict of interest.

Acknowledgements

This work is supported by the U.S. Department of Energy, Office of Fossil Energy, under Award Number DE-FE0026463 and the U.S. National Science Foundation (NSF) grant number 1804996.

References

1 J. O. Abe, A. P. I. Popoola, E. Ajenifuja and O. M. Popoola, *Int. J. Hydrogen Energy*, 2019, 44, 15072–15086.

2 N. Z. Muradov and T. N. Veziroğlu, *Int. J. Hydrogen Energy*, 2005, **30**, 225–237.

3 S. Kishore, J. A. Nelson, J. H. Adair and P. C. Eklund, *J. Alloys Compd.*, 2005, **389**, 234–242.

4 B. D. Adams and A. Chen, *Mater. Today*, 2011, 14, 282–289.

5 T. B. Flanagan and W. A. Oates, *Annu. Rev. Mater. Sci.*, 1991, **21**, 269–304.

6 M. R. Rahimpour, F. Samimi, A. Babapoor, T. Tohidian and S. Mohebi, *Chem. Eng. Process. Process Intensif.*, 2017, **121**, 24–49.

7 N. A. Al-Mufachi, N. V. Rees and R. Steinberger-Wilkens, *Renew. Sustain. Energy Rev.*, 2015, **47**, 540–551.

8 L. C. Liu, J. W. Wang, Y. H. He and H. R. Gong, *J. Memb. Sci.*, 2017, **542**, 24–30.

9 N. Endo, Y. Furukawa, K. Goshome, S. Yaegashi, K. ichi Mashiko and M. Tetsuhiko, *Int. J. Hydrogen Energy*, 2019, **44**, 8290–8297.

10 E. Acha, Y. C. van Delft, J. F. Cambra and P. L. Arias, *Chem. Eng. Sci.*, 2018, **176**, 429–438.
11 C. P. O'Brien and I. C. Lee, *Catal. Today*, 2019, **336**, 216–222.
12 L. Zhao, A. Goldbach and H. Xu, *J. Memb. Sci.*, 2016, **507**, 55–62.
13 K. Zhang and J. D. Way, *Sep. Purif. Technol.*, 2017, **186**, 39–44.
14 G. Zeng, A. Goldbach, L. Shi and H. Xu, *Int. J. Hydrogen Energy*, 2012, **37**, 6012–6019.
15 S. Nayebossadri, J. D. Speight and D. Book, *Int. J. Hydrogen Energy*, 2019, **44**, 29092–29099.
16 C. H. Chen, Y. R. Huang, C. W. Liu and K. W. Wang, *Thin Solid Films*, 2016, **618**, 189–194.
17 S. Barison, S. Fasolin, S. Boldrini, A. Ferrario, M. Romano, F. Montagner, S. M. Deambrosis, M. Fabrizio and L. Armelao, *Int. J. Hydrogen Energy*, 2018, **43**, 7982–7989.
18 A. M. Tarditi, F. Braun and L. M. Cornaglia, *Appl. Surf. Sci.*, 2011, **257**, 6626–6635.
19 F. Pişkin and T. Öztürk, *J. Memb. Sci.*, 2017, **524**, 631–636.
20 S. K. Ryi, J. S. Park, S. H. Kim, D. W. Kim and K. Il Cho, *J. Memb. Sci.*, 2008, **318**, 346–354.
21 H. Lin, E. Van Wagner, B. D. Freeman, L. G. Toy and R. P. Gupta, *Science.*, 2006, **311**, 639–642.
22 L. Hu, S. Pal, H. Nguyen, V. Bui and H. Lin, *J. Polym. Sci.*, 2020, **58**, 2467–2481.
23 M. J. C. Ordoñez, K. J. Balkus, J. P. Ferraris and I. H. Musselman, *J. Memb. Sci.*, 2010, **361**, 28–37.
24 A. C. Puleo, D. R. Paul and S. S. Kelley, *J. Memb. Sci.*, 1989, **47**, 301–332.
25 J. S. McHattie, W. J. Koros and D. R. Paul, *Polymer*, 1991, **32**, 2618–2625.
26 Z. P. Smith, R. R. Tiwari, T. M. Murphy, D. F. Sanders, K. L. Gleason, D. R. Paul and B. D. Freeman, *Polymer*, 2013, **54**, 3026–3037.
27 K. A. Berchtold, R. P. Singh, J. S. Young and K. W. Dudeck, *J. Memb. Sci.*, 2012, **415–416**, 265–270.
28 L. Zhu, D. Yin, Y. Qin, S. Konda, S. Zhang, A. Zhu, S. Liu, T. Xu, M. T. Swihart and H. Lin, *Adv. Funct. Mater.*, 2019, **29**, 1904357.
29 H. S. M. Suhaimi, C. P. Leo and A. L. Ahmad, *Chem. Eng. Technol.*, 2017, **40**, 631–638.
30 A. Kumar, M. M. Mohammadi and M. T. Swihart, *Nanoscale*, 2019, **11**, 19058–19085.
31 Y. Wang, S.-I. Choi, X. Zhao, S. Xie, H.-C. Peng, M. Chi, C. Z. Huang and Y. Xia, *Adv. Funct. Mater.*, 2014, **24**, 131–139.
32 J. J. Conde, M. Maroño and J. M. Sánchez-Hervás, *Sep. Purif. Rev.*, 2017, **46**, 152–177.
33 L. Zhu, M. T. Swihart and H. Lin, *J. Mater. Chem. A*, 2017, **5**, 19914–19923.
34 F. Li, Y. Ji, S. Wang, S. Li and Y. Chen, *Electrochim. Acta*, 2015, **176**, 125–129.
35 Y. Gong, X. Liu, Y. Gong, D. Wu, B. Xu, L. Bi, L. Y. Zhang and X. S. Zhao, *J. Colloid Interface Sci.*, 2018, **530**, 189–195.
36 M. B. Lim, J. L. Hanson, L. Vandsburger, P. B. Roder, X. Zhou, B. E. Smith, F. S. Ohuchi and P. J. Pauzauskie, *J. Mater. Chem. A*, 2018, **6**, 5644–5651.
37 K. M. Koczkur, S. Mourdikoudis, L. Polavarapu and S. E. Skrabalak, *Dalt. Trans.*, 2015, **44**, 17883–17905.
38 S. S. Batsanov, *Inorg. Mater.*, 2001, **37**, 871–885.
39 D. Bin, B. Yang, F. Ren, K. Zhang, P. Yang and Y. Du, *J. Mater. Chem. A*, 2015, **3**, 14001–14006.
40 B. Yan, H. Xu, K. Zhang, S. Li, J. Wang, Y. Shi and Y. Du, *Appl. Surf. Sci.*, 2018, **434**, 701–710.
41 Y. Lu and W. Chen, *ACS Catal.*, 2012, **2**, 84–90.
42 M. H. Seo, S. M. Choi, J. K. Seo, S. H. Noh, W. B. Kim and B. Han, *Appl. Catal. B Environ.*, 2013, **129**, 163–171.
43 G. Dong, H. Li and V. Chen, *J. Mater. Chem. A*, 2013, **1**, 4610–4630.
44 H. Lin, Z. He, Z. Sun, J. Vu, A. Ng, M. Mohammed, J. Kniep, T. C. Merkel, T. Wu and R. C. Lambrecht, *J. Memb. Sci.*, 2014, **457**, 149–161.